



Cite this: *RSC Adv.*, 2025, **15**, 16164

## Upcycling waste zirconia block dental powders: towards a facile and highly selective on-off optical probe for sensing $Zn^{2+}$ and $Hg^{2+}$ in aqueous media<sup>†</sup>

Amin Moghaddasfar, <sup>a</sup> Ghodsi Mohammadi Ziarani <sup>b</sup> and Alireza Badiei <sup>\*a</sup>

Upcycling waste materials to produce high-value-added substances can pave the way for sustainable development. Waste block dental powders (WBDPs), a valuable source of zirconia, represent a significant portion of dentistry wastage and are valuable candidates for upcycling. Herein, a highly selective and facile optical probe based on upcycled WBDPs with surface interaction of 8-hydroxyquinoline-5-sulfonate (8-HQS) was developed to produce a powerful solid-state optical chemo-probe for sensing  $Zn^{2+}$  and  $Hg^{2+}$  in aqueous media.  $ZrO_2$ -8-HQS provided high selectivity for sensing  $Zn^{2+}$  over a wide range of cations and anions, with a remarkable fluorescence intensity enhancement ( $\lambda_{em} = 517$  nm) over a wide pH range (4–10). The as-prepared optical probe had a remarkable sensitivity, with a limit of detection (LoD) of 5.2  $\mu$ M for  $Zn^{2+}$ . The fluorescence of the  $Zn^{2+}$  probe complex was quenched in the presence of aqueous solutions of  $Hg^{2+}$ , allowing the as-prepared chemo-probe to sense  $Hg^{2+}$  in aqueous media (LoD of 0.8  $\mu$ M for  $Hg^{2+}$ ). The Stern–Volmer equation revealed static and dynamic mechanisms in the quenching process, and the ( $K_S \times K_D$ ) and ( $K_S + K_D$ ) values were 0.0012 and 0.0076, respectively.

Received 10th March 2025

Accepted 16th April 2025

DOI: 10.1039/d5ra01728a

rsc.li/rsc-advances

### 1. Introduction

Upcycling of waste materials is a promising method to convert them into high-value-added substances in their second life.<sup>1,2</sup> In the past few decades, with the development of industries, a wide range of high-value inorganic solids have been produced for use in various sectors. However, significant amounts of these materials have been wasted and have not been recycled or upcycled. The development of a recycling or upcycling system for inorganic solid wastes is one of the important issues that help to continue environmentally sustainable development in the future.<sup>3</sup> For instance, Badiei's group<sup>4</sup> recycled e-waste tantalum and PET waste to synthesize an upcycled metal-organic framework as an optical chemo-sensor for the detection of chloroacetaldehyde.

One of the inorganic solids is yttria tetragonal zirconia (YTZ), which has attracted attention as a promising material for dentistry. It is mainly used for building prosthodontics due to its biocompatibility, mechanical strength, and excellent esthetic properties.<sup>5</sup> The utilization of computer-aided design/computer-aided manufacturing (CAD/CAM) technology allows dental laboratories and clinicians to manufacture dental

restorations with precision and efficiency. However, the CAD/CAM milling process results in up to 80% of waste from the original disc's or block's bulk due to indirect milling of restoration. During this process, 30% of the waste becomes powder, while up to 50% remains unused, leading to noticeable environmental and economic losses.<sup>6</sup> Nowadays, residual dental YTZ has been recycled by some companies. Unfortunately, the recycled YTZ has an irregular shape and a larger particle size, which can negatively impact its molding and sintering kinetics.<sup>7</sup>

In the last decade, human civilization development has rapidly increased water pollution.<sup>8,9</sup> Conventional detection techniques such as GC, LC, and HPLC are limited by some shortcomings. The drawbacks of traditional methods are that some cannot detect low levels of harmful pollutants in water, especially free metal ions, and are costly, inaccessible, and complicated.<sup>10,11</sup> Recently, fluorescence chemo-probes have been developed as a powerful method for sensing a wide range of metal ions, due to their high sensitivity, simplicity, selectivity, and on-site detection. Among the chemo-probes, some normally have a receptor that selectively interacts with the specific contaminant and a fluorophore that translates the molecular recognition into a fluorescence signal.<sup>12–14</sup> Selective detection of transition metal ions has attracted the attention of researchers due to their fundamental effects on environmental, medical, and biological processes. Among metal ions, zinc ion (as a d<sup>10</sup> metal ion) cannot effectively be detected by conventional methods such as absorption spectroscopy.<sup>15,16</sup> Behind iron, zinc ( $Zn^{2+}$ ), the second most essential and abundant

<sup>a</sup>School of Chemistry, College of Sciences, University of Tehran, Iran. E-mail: abadiei@ut.ac.ir

<sup>b</sup>Department of Organic Chemistry, Faculty of Chemistry, Alzahra University, Iran

† Electronic supplementary information (ESI) available. See DOI: <https://doi.org/10.1039/d5ra01728a>

transition element in the human body, plays a crucial role in biological processes, including gene transcription, brain function, signal transmission, and mammalian reproduction.<sup>17,18</sup> A wide range of  $Zn^{2+}$  fluorescence sensors have been developed based on various mechanisms including internal charge transfer (ICT),<sup>19</sup> excimer/exciplex formation and extinction,<sup>20</sup> photoinduced electron transfer (PET),<sup>21</sup> and fluorescence resonance energy transfer (FRET).<sup>22</sup> However, some of them also respond to other metal ions such as  $Pb^{2+}$ ,  $Cd^{2+}$ ,  $Ni^{2+}$ , and  $Co^{2+}$ . Therefore, researchers still desire to develop novel optical chemo-probes with selective high affinity for  $Zn^{2+}$  over other relevant metal ions. Mercury ( $Hg^{2+}$ ) is also a hazardous heavy metal ion that is discharged into water because of human industrial activity developments, leading to environmental pollution that can adversely affect human health.<sup>23-25</sup> Therefore, the development of a facile and selective optical probe for sensing  $Zn^{2+}$  and  $Hg^{2+}$  in aqueous media is very essential for the development of human civilization.<sup>26,27</sup>

One of the most promising compounds for this purpose is the use of 8-hydroxyquinoline-5-sulfonate (8-HQS) and its derivatives due to their affinity and chelating interaction towards a wide range of metal ions and the high luminescence efficiency of the resulting metal complexes.<sup>28,29</sup> As a ligand, it exhibits weak fluorescence activity primarily due to an intramolecular proton ( $H^+$ ) transfer from oxygen to nitrogen in the excited state, leading to a non-radiative relaxation pathway. The interaction of 8-HQS with a wide range of metal ions can result in hydroxyl  $H^+$  replacement with metal ions and consequently suppress the intramolecular  $H^+$  transfer.<sup>30</sup> Therefore, the chelation of metal ions to 8-HQS produces a solid-state probe, bestowing it with significant enhancement in the emission intensity. According to research, zirconia ( $ZrO_2$ ) presumably interacts with the sulfonic acid head of 8-HQS, for which two scenarios are possible: tripodal and chelating configuration.<sup>31</sup>

Furthermore,  $Zn^{2+}$  presumably bonds to 8-HQS through the nitrogen and oxygen donor atoms.<sup>32-34</sup>

This study, to the best of our knowledge, is the first attempt to upcycle WBDPs with 8-HQS as a powerful solid-state optical chemo-probe. The result revealed that  $ZrO_2$  nanoparticles (NPs) could successfully enhance the PL properties of 8-HQS for the sensing of  $Zn^{2+}$  ions. The PL properties, stability in a wide pH range, particle size distribution, and zeta potential of the as-prepared solid-state optical probe were investigated. The quenching of emission intensity in the presence of  $Hg^{2+}$  allows the  $Zn^{2+}$  optical probe complex to sense  $Hg^{2+}$  in aqueous media. The quenching mechanism was evaluated by the Stern–Volmer equation and illustrated static and dynamic mechanisms in the quenching process.

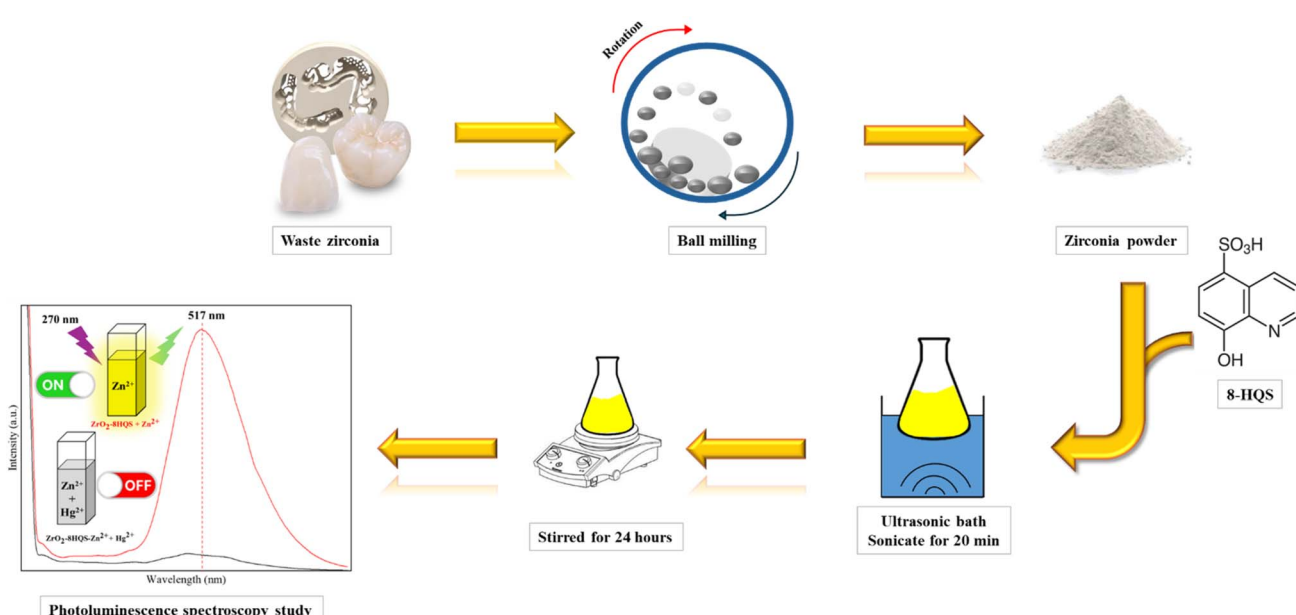
## 2. Experimental section

### 2.1. Chemicals

The chemicals used in this study are waste zirconia block, 8-HQS (Merck), sodium hydroxide (NaOH, Sigma), hydrochloric acid (HCl, Sigma), nitrate salts of the metal cations ( $K^+$ ,  $Ag^+$ ,  $Hg^+$ ,  $Ni^{2+}$ ,  $Mn^{2+}$ ,  $Cd^{2+}$ ,  $Ca^{2+}$ ,  $Pb^{2+}$ ,  $Fe^{2+}$ ,  $Mg^{2+}$ ,  $Cu^{2+}$ ,  $Zn^{2+}$ ,  $Hg^{2+}$ ,  $Cr^{3+}$ ,  $Fe^{3+}$ , and  $Al^{3+}$ ) and sodium salts of anions ( $I^-$ ,  $Br^-$ ,  $Cl^-$ ,  $NO_3^-$ ,  $NO_2^-$ ,  $CH_3COO^-$ ,  $MoO_4^{2-}$ ,  $CO_3^{2-}$ ,  $Cr_2O_7^{2-}$ ,  $SO_4^{2-}$ ,  $S_2O_3^{2-}$  and  $SCN^-$ ). All the above-mentioned compounds were of HPLC-reagent grade and used without any further purification.

### 2.2. Characterization techniques

For Fourier-transform infrared (FTIR) spectroscopy measurement of  $ZrO_2$  NPs, Rayleigh WQF-510A (China) was used. A tablet mixture of  $ZrO_2$  NPs and potassium bromide (KBr) was scanned in the range of  $4000\text{ cm}^{-1}$  to  $400\text{ cm}^{-1}$  with 9 scans. The X-ray diffraction (XRD) pattern to determine the



**Scheme 1** Schematic of the preparation of  $ZrO_2$ -8-HQS as an on-off optical chemo-probe for sensing  $Zn^{2+}$  and  $Hg^{2+}$ .



crystallinity and phase of the  $\text{ZrO}_2$  NPs was recorded using a Rigaku Ultima IV (Belgium) instrument (the characterization was done at ambient temperature ( $\text{K}\alpha$  X-ray of Cu was used)). Scanning electron microscopy (SEM) was performed using a MIRA3-Tescan for morphology investigation. The Raman spectrum was studied using a Teksan N1-541 instrument (Nd:YAG laser source,  $\lambda = 785$  nm/Iran). To find the optical properties of the as-prepared chemo probe, a UV-vis spectrophotometer (Raleigh UV-1600/China) and a PL spectrometer (Agilent-G980A/USA) were used. Horiba SZ-100 was used for dynamic light scattering (DLS) and zeta potential to estimate

the particle size of  $\text{ZrO}_2$ -8-HQS and  $\text{ZrO}_2$  and to confirm the interaction between HQS and  $\text{ZrO}_2$  in the liquid phase, respectively.

### 2.3. Suspension preparation and photoluminescence property examination

The WBDP ball milling was used to achieve a fine  $\text{ZrO}_2$  NPs powder. To activate the  $\text{ZrO}_2$  NP surface, 0.03 g of the obtained  $\text{ZrO}_2$  NPs were dispersed in 50 mL of distilled water and sonicated in an ultrasonic bath for 20 min. Then, 0.01 g of 8-HQS was dissolved in 50 mL of water and poured into the  $\text{ZrO}_2$ -activated suspension. The obtained suspension was sonicated for 20 min and then stirred for 24 hours (Scheme 1). For PL studies, 2 mL of prepared suspension was poured into a cuvette. Subsequently, 5  $\mu\text{L}$  of different cations and anions ( $10^{-2}$  M) was added to examine the chemo-sensitivity of the as-prepared probe. The pH of the solution was adjusted by utilizing the desired volumes of HCl and NaOH solutions.

## 3. Results and discussion

### 3.1. Characterization of $\text{ZrO}_2$ NPs and $\text{ZrO}_2$ -8-HQS

The XRD analysis obtained from  $\text{ZrO}_2$  NPs revealed that the particles are highly pure and crystalline (Fig. 1a). The deflection peaks revealed sharp and high intensity. The XRD obtained result confirms the dominance of the tetragonal phase of  $\text{ZrO}_2$  NPs over the monoclinic phase (JCPDS cards no. 17-0923 and 37-1484). The positions of the deflections corresponding to the monoclinic phase were (110), ( $-111$ ), (111), (002), ( $-012$ ), ( $-211$ ), ( $-202$ ), (022), (221), ( $-231$ ), and ( $-041$ ), while the

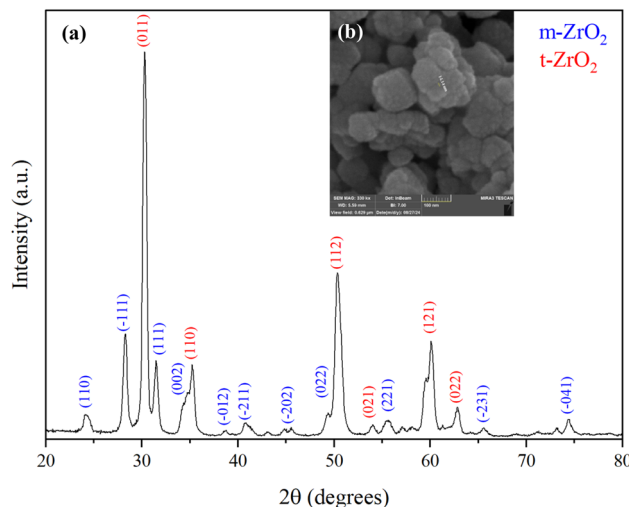


Fig. 1 (a) XRD pattern and (b) SEM image of  $\text{ZrO}_2$  NPs prepared from WBDPs.

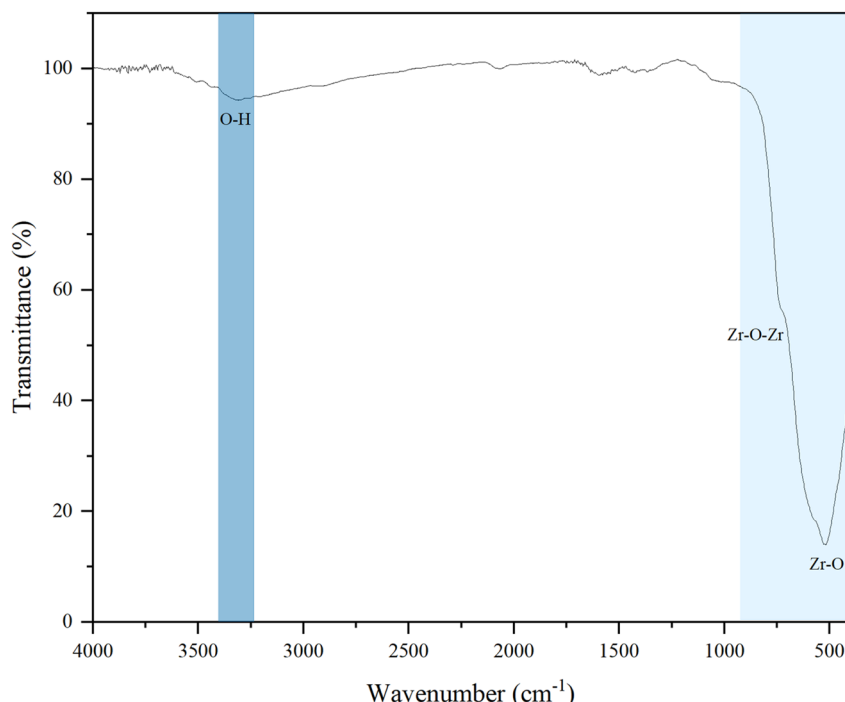


Fig. 2 FTIR spectrum of  $\text{ZrO}_2$  NPs prepared from WBDPs.



positions corresponding to the tetragonal phase were (011), (110), (112), (021), (121), and (022). Furthermore, the crystallite size of the  $\text{ZrO}_2$  NPs was estimated from the XRD data using the Scherrer equation given in eqn (1):

$$D = \frac{k\lambda}{\beta \cos \theta} \quad (1)$$

In this context, the size of the crystallite is represented as  $D$ , where  $k = 0.89$  denotes a correction particle shape factor. The full width at half maximum (FWHM) is represented as  $\beta$ , the

wavelength of the Cu target is  $1.54 \text{ \AA}$  and is represented as  $\lambda$ , and the Bragg angle is represented as  $\theta$ . The average crystallite size was calculated to be  $16.55 \text{ nm}$  using the Debye–Scherrer equation.

The SEM characterization of the as-prepared  $\text{ZrO}_2$  NPs is illustrated in Fig. 1b. The SEM result reveals the aggregation of NPs. Furthermore, it confirmed a uniform morphology of the as-prepared NPs, and the particle size was estimated using the Digimizer software and obtained as about  $14 \text{ nm}$ . The Fourier transform infrared (FTIR) spectra recorded in the range of  $4000\text{--}400 \text{ cm}^{-1}$  are presented in Fig. 2. In the fingerprint region at  $900\text{--}500 \text{ cm}^{-1}$ , the transmittance peak at  $733 \text{ cm}^{-1}$  corresponds to the  $\text{Zr}=\text{O}=\text{Zr}$  vibration bond. The peak at  $523 \text{ cm}^{-1}$  exhibits a  $\text{Zr}=\text{O}$  peak. To distinguish the structure of  $\text{ZrO}_2$ , the Raman spectra of  $\text{ZrO}_2$  are displayed in Fig. 3. The vibration bonds of m- $\text{ZrO}_2$  appeared at  $170$ ,  $366$ , and  $544 \text{ cm}^{-1}$ . Meanwhile, the vibration bonds of t- $\text{ZrO}_2$  appeared at  $135$ ,  $247$ ,  $316$ ,  $461$ , and  $625 \text{ cm}^{-1}$ .<sup>35</sup>

The DLS results of  $\text{ZrO}_2$ -8-HQS are shown in Fig. S1.<sup>†</sup> According to these results, some NPs successfully interacted with 8-HQS, forming complexes of  $23.1 \text{ nm}$ , while others remain dispersed as  $\text{ZrO}_2$  NPs in water, measuring  $16.1 \text{ nm}$ . This behavior can be clarified by the formation of coordination complexes between the  $\text{ZrO}_2$  NPs and 8-HQS. It is pertinent to mention that the PL properties obtained from DLS analysis confirm this interaction. As indicated in Table 1, the PL properties of  $\text{ZrO}_2$  NPs interacting with 8-HQS show a remarkable increase in emission intensity compared to  $\text{ZrO}_2$  NPs alone. Additionally, the DLS peak of  $\text{ZrO}_2$  NPs is sharp, whereas the DLS peak of  $\text{ZrO}_2$ -8-HQS is broader. This phenomenon is attributed to the uniform hydrodynamic radius around  $\text{ZrO}_2$  NPs. However, the interaction between 8-HQS and the  $\text{ZrO}_2$  network is not uniform, resulting in a non-uniform hydrodynamic radius and a broad non-uniform DLS peak for  $\text{ZrO}_2$ -8-HQS.

The zeta potential of  $\text{ZrO}_2$ -8-HQS, as shown in Fig. S2,<sup>†</sup> revealed a negative charge of  $-0.3 \text{ mV}$ , indicating the successful interaction of 8-HQS with  $\text{ZrO}_2$  NPs.

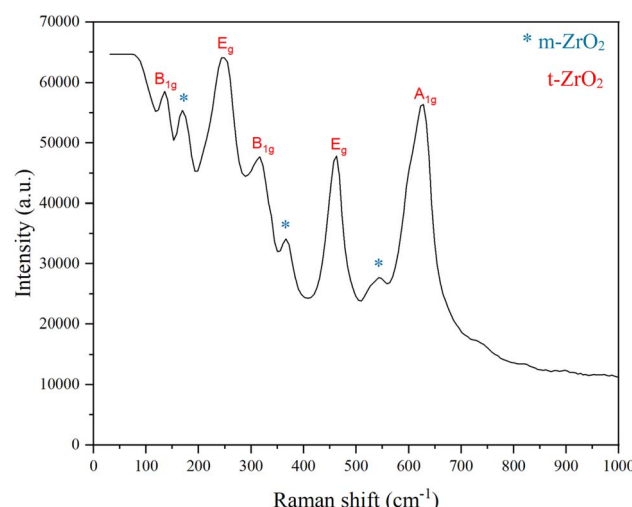


Fig. 3 Raman spectrum of  $\text{ZrO}_2$  NPs prepared from WBDPs.

Table 1 DLS results of  $\text{ZrO}_2$  NPs and  $\text{ZrO}_2$ -8-HQS

| Sample                | Hydrodynamic radius (nm) | PL    |
|-----------------------|--------------------------|-------|
| $\text{ZrO}_2$        | 16.1                     | 0.076 |
| $\text{ZrO}_2$ -8-HQS | 23.1                     | 0.230 |

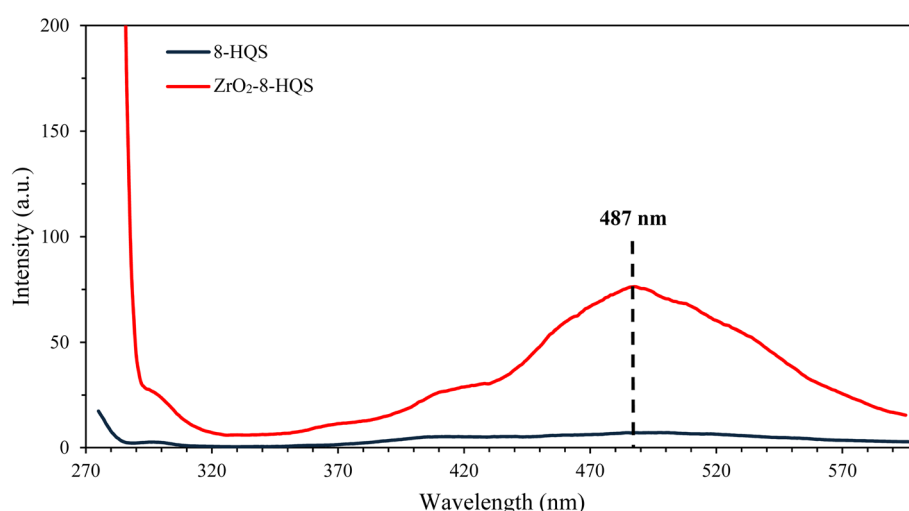


Fig. 4 Fluorescence emission comparison of 8-HQS (dark blue line) and  $\text{ZrO}_2$ -8-HQS (red line) ( $\lambda_{\text{ex}} = 270 \text{ nm}$ ).



### 3.2. Photoluminescence examination

**3.2.1.  $\text{ZrO}_2$ -8-HQS as a sensory probe for  $\text{Zn}^{2+}$ .** Optical chemo-probe gained scientific attention due to their promising advantages compared to the conventional methods. To visualize the performance of  $\text{ZrO}_2$ -8-HQS as the optical chemo-probe, a wide range of anions and cations were used to estimate its selectivity and sensitivity. For all PL analyses, 2 mL of  $\text{ZrO}_2$ -8-HQS was poured into the cuvette, and the excitation wavelength

was adjusted at 270 nm ( $\lambda_{\text{ex}} = 270 \text{ nm}$ ). The PL studies of 8-HQS and  $\text{ZrO}_2$  bonded to 8-HQS ( $\text{ZrO}_2$ -8-HQS) are illustrated in Fig. 4. The PL results showed an enhancement in the emission intensity of  $\text{ZrO}_2$ -8-HQS at 487.01 nm. According to research, zirconia bonded with the sulfuric acid head of 8-HQS.<sup>36</sup>

To evaluate the selectivity of the as-prepared chemo-probe for sensing ions in water, 2 mL of  $\text{ZrO}_2$ -8-HQS was poured into the cuvette, followed by the addition of 5  $\mu\text{L}$  of various

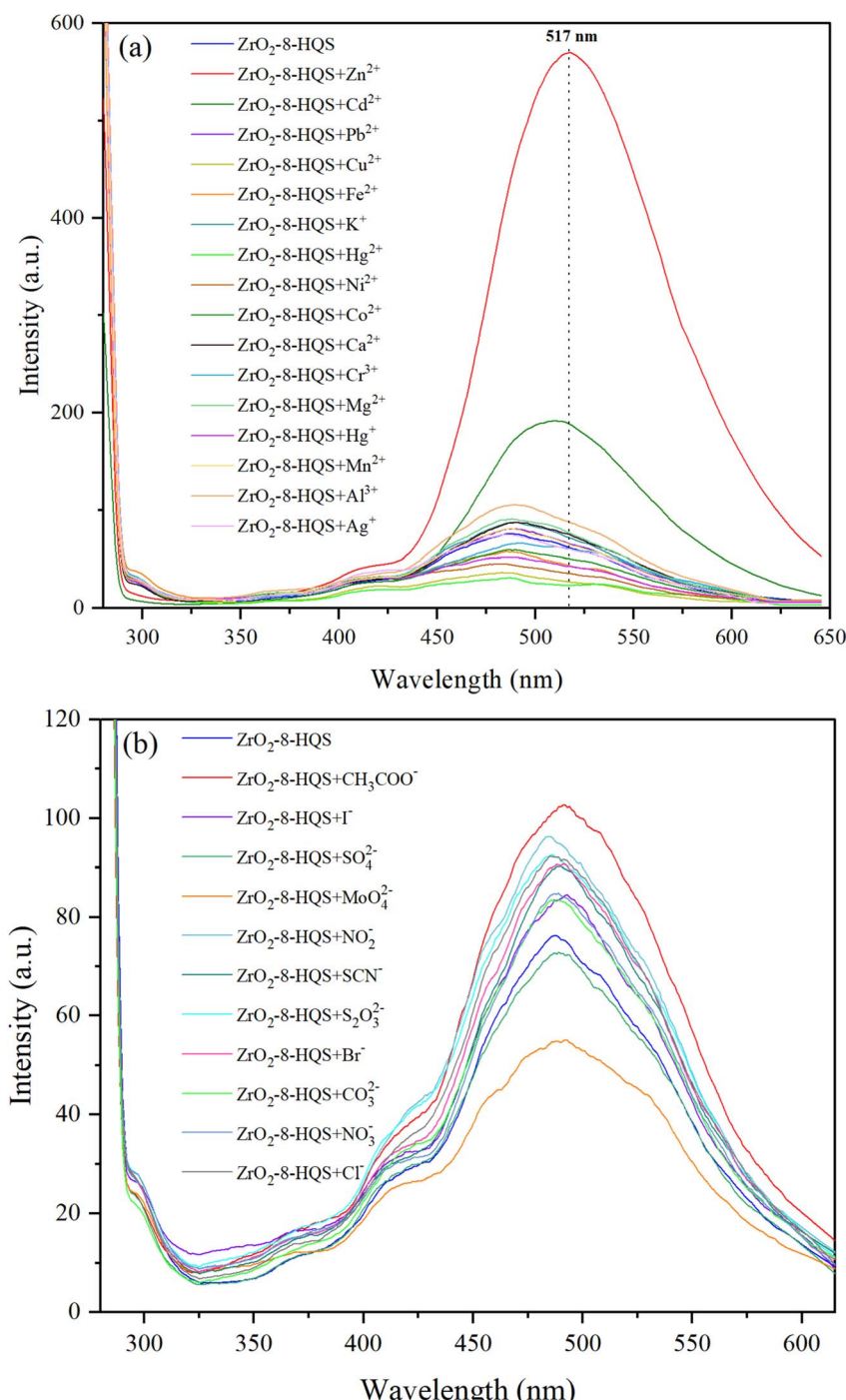
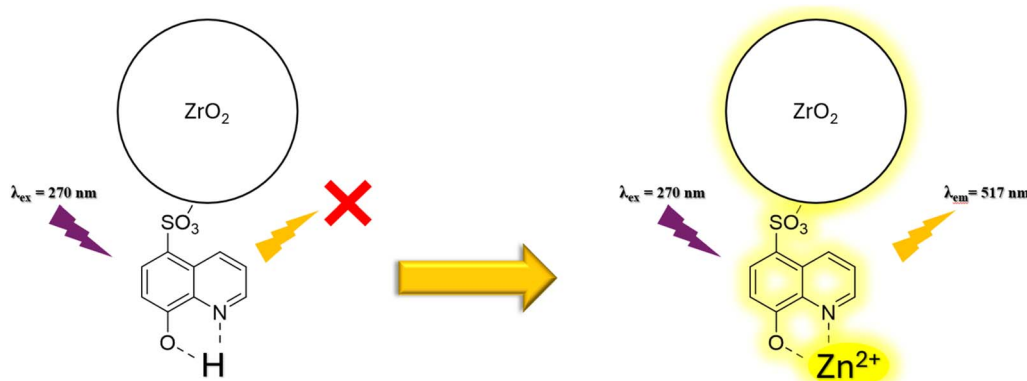
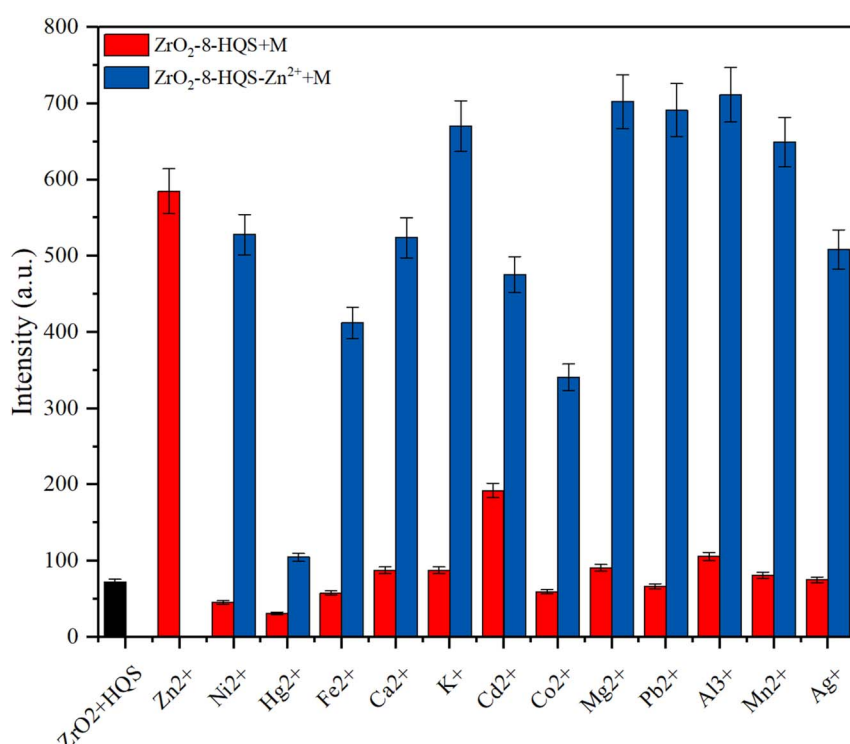


Fig. 5 Fluorescence emission of  $\text{ZrO}_2$ -8-HQS in the presence of (a) metal ions including  $\text{K}^+$ ,  $\text{Ag}^+$ ,  $\text{Ni}^{2+}$ ,  $\text{Mn}^{2+}$ ,  $\text{Cd}^{2+}$ ,  $\text{Ca}^{2+}$ ,  $\text{Pb}^{2+}$ ,  $\text{Fe}^{2+}$ ,  $\text{Co}^{2+}$ ,  $\text{Mg}^{2+}$ ,  $\text{Cu}^{2+}$ ,  $\text{Zn}^{2+}$ ,  $\text{Hg}^{2+}$ ,  $\text{Cr}^{3+}$ ,  $\text{Fe}^{3+}$ , and  $\text{Al}^{3+}$  and (b) anions including  $\text{I}^-$ ,  $\text{Br}^-$ ,  $\text{Cl}^-$ ,  $\text{NO}_3^-$ ,  $\text{NO}_2^-$ ,  $\text{CH}_3\text{COO}^-$ ,  $\text{MoO}_4^{2-}$ ,  $\text{CO}_3^{2-}$ ,  $\text{SO}_4^{2-}$ ,  $\text{S}_2\text{O}_3^{2-}$  and  $\text{SCN}^-$  ( $\lambda_{\text{ex}} = 270 \text{ nm}$ ).



Scheme 2 Mechanistic pathway of the  $\text{ZrO}_2$ -8-HQS for the sensing of  $\text{Zn}^{2+}$ .Table 2 Comparison of different studies to detect  $\text{Zn}^{2+}$ 

| Sensor   | LoD (M)               | Measured signal | Reference  |
|--|-----------------------|-----------------|------------|
| 4-Methyl-2,6-bis((E)-(2-(phthalazin-1-yl)hydrazone)methyl)phenol   | $2.3 \times 10^{-6}$  | Fluorescence    | 38         |
| (E)-1-((2-(9-(Naphthalen-1-yl)-8-(thiophen-2-yl)-9H-purin-6-yl)hydrazone)methyl)naphthalen 2-ol          | $6.1 \times 10^{-8}$  | Fluorescence    | 39         |
| 2-(Pyridin-2-yl)-4,7-di(thiophen-2-yl)-3H-benzo[d]imidazole  | $1.6 \times 10^{-8}$  | Fluorescence    | 40         |
| 3-[1-(4-Dimethylamino)phenylimino]ethyl 4-hydroxy-2H-chromen-2-one                                       | $6.5 \times 10^{-5}$  | Fluorescence    | 41         |
| 7-(2',4'-Dihydroxy benzylidene amino)-4-methylcoumarin   | $3.8 \times 10^{-6}$  | Fluorescence    | 42         |
| Dipicolinohydrazonamide  | $24 \times 10^{-6}$   | Fluorescence    | 43         |
| 4,4'-(Propane-2,2-diyl)bis(2-(((2morpholinoethyl)imino)methyl)phenol)                                    | $7.05 \times 10^{-8}$ | Fluorescence    | 44         |
| (E)-2-((2-(2,4-Dinitrophenyl)hydrazineylidene) methyl)phenol   | $1.1 \times 10^{-8}$  | Fluorescence    | 45         |
| (E)-3,5-Di- <i>tert</i> -butyl-2-hydroxy- <i>N'</i> -((1-hydroxynaphthalen-2-yl)methylene)benzohydrazide | $2.2 \times 10^{-9}$  | Fluorescence    | 46         |
| 2-(Benzod[d]thiazol-2-yl)-6-(1-(pyridin-2-yl)imidazo[1,5- <i>a</i> ] pyridin-3-yl) phenol                | $2.36 \times 10^{-8}$ | Fluorescence    | 47         |
| $\text{ZrO}_2$ -8-HQS  | $5.2 \times 10^{-6}$  | Fluorescence    | This study |

Fig. 6 Effect of various metal ions on the  $\text{ZrO}_2$ -8-HQS +  $\text{Zn}^{2+}$  emission intensity.

metal ions and anions (the concentration of all metal ions and anions adjusted at  $10^{-2}$  M). Fig. 5 reveals the response of the chemo-probe to different metal ions and anions. Compared to other metal ions, the emission intensity was enhanced for  $\text{Al}^{3+}$ ,  $\text{Cd}^{2+}$ , and  $\text{Ag}^+$ , while other ions caused quenching. Upon the addition of  $\text{Zn}^{2+}$ , the emission intensity was remarkably enhanced and showed a red shift from 487.01 nm to

517.951 nm. Jianbo and co-workers<sup>34</sup> reported that  $\text{Zn}^{2+}$  interacts with oxygen and nitrogen groups of 8-HQ and produces 8-HQ zinc complexes that suppress the intramolecular  $\text{H}^+$  transfer (Scheme 2). The absorption spectroscopy results (Fig. S3†) clearly indicated a blue shift after the interaction of  $\text{Zn}^{2+}$  with the as-prepared solid-state optical probe, leading to an ICT mechanism.<sup>37</sup> According to Fig. S4,† the LoD of sensing  $\text{Zn}^{2+}$

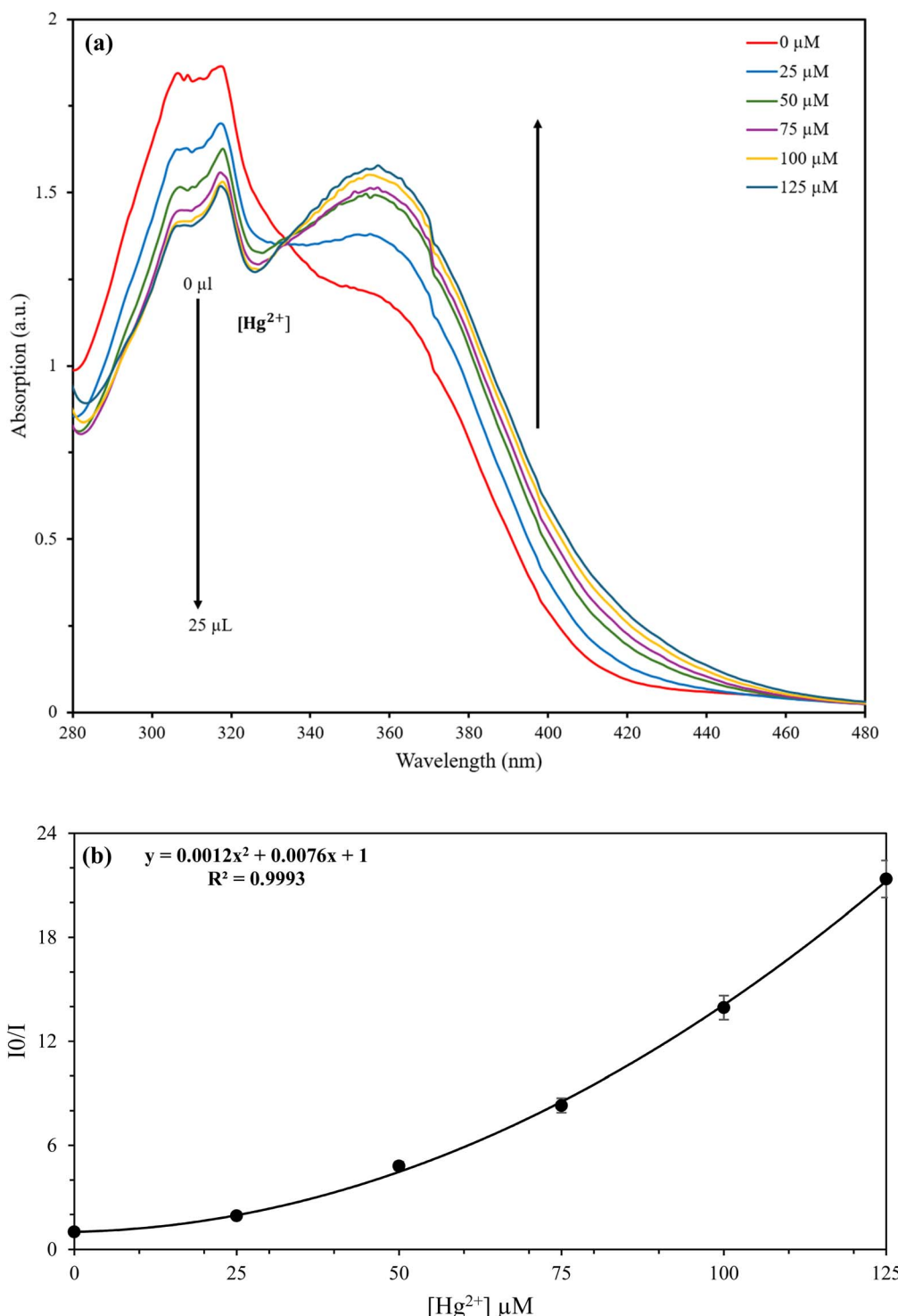


Fig. 7 (a) Titration plot of  $\text{ZrO}_2$ -8-HQS- $\text{Zn}^{2+}$  through the addition of  $\text{Hg}^{2+}$ . (b) Non-linear modified Stern–Volmer quenching plot.



Table 3 Comparison of different studies to detect  $\text{Hg}^{2+}$ 

| Sensor   | LoD (M)               | Measured signal | Reference  |
|--|-----------------------|-----------------|------------|
| rGO@MoS <sub>2</sub>   | $2.3 \times 10^{-9}$  | Fluorescence    | 49         |
| S <sub>x</sub> N-GQDs  | $9.1 \times 10^{-6}$  | Fluorescence    | 50         |
| Tetra( <i>p</i> -dimethylaminophenyl)porphyrin                         | $8.0 \times 10^{-9}$  | Fluorescence    | 51         |
| CNPs-RhB nanohybrid  | $4.2 \times 10^{-8}$  | Fluorescence    | 52         |
| PET-CHEF-FRET  | $1.5 \times 10^{-10}$ | Fluorescence    | 53         |
| Rhodamine pyrene conjugate   | $1.9 \times 10^{-5}$  | Fluorescence    | 54         |
| 2-(Rhodamine- <i>b</i> -hydrazido)- <i>N</i> -(quinolin-8-yl)acetamide | $4.5 \times 10^{-7}$  | Fluorescence    | 55         |
| NETBZ  | $1.4 \times 10^{-8}$  | Fluorescence    | 56         |
| ZrO <sub>2</sub> -8-HQS-Zn   | $8.04 \times 10^{-7}$ | Fluorescence    | This study |

was calculated as  $5.2 \mu\text{M}$ . The response time of the as-prepared chemo probe interacting with  $\text{Zn}^{2+}$  was evaluated, and is shown in Fig. S5.† The results indicated that the interaction of ZrO<sub>2</sub>-8-HQS occurred rapidly within the first 10 seconds, and no noticeable change in emission intensity was observed afterward, even when the duration was extended to 300 seconds. Table 2 demonstrates the compression of various studies to detect  $\text{Zn}^{2+}$  with this work.

**3.2.2. Effects of competitive metal ions.** The presence of a wide range of interfering ions in environments can affect chemo-probe response. In this regard, metal ions including  $\text{Ni}^{2+}$ ,  $\text{Hg}^{2+}$ ,  $\text{Fe}^{2+}$ ,  $\text{Ca}^{2+}$ ,  $\text{K}^+$ ,  $\text{Cd}^{2+}$ ,  $\text{Co}^{2+}$ ,  $\text{Mg}^{2+}$ ,  $\text{Pb}^{2+}$ ,  $\text{Al}^{3+}$ ,  $\text{Mn}^{2+}$ , and  $\text{Ag}^+$  were added to the mixture of ZrO<sub>2</sub>-8-HQS +  $\text{Zn}^{2+}$  for competitive study examination (Fig. 6). The results indicated that ZrO<sub>2</sub>-8-HQS +  $\text{Zn}^{2+}$  showed no significant change in emission intensity in the presence of  $\text{Ni}^{2+}$ ,  $\text{Ca}^{2+}$ ,  $\text{Cd}^{2+}$ ,  $\text{Mn}^{2+}$ , and  $\text{Ag}^+$ . However, the emission intensity was slightly enhanced by the presence of  $\text{K}^+$ ,  $\text{Mg}^{2+}$ ,  $\text{Pb}^{2+}$ , and  $\text{Al}^{3+}$ . In contrast, the addition of  $\text{Co}^{2+}$  and  $\text{Fe}^{2+}$  caused a negligible quenching of the emission intensity of ZrO<sub>2</sub>-8-HQS +  $\text{Zn}^{2+}$ . Notably, the addition of  $\text{Hg}^{2+}$  completely quenched the emission intensity.

**3.2.3. ZrO<sub>2</sub>-8-HQS +  $\text{Zn}^{2+}$  as a sensory probe for  $\text{Hg}^{2+}$ .** Through the competitive investigation,  $\text{Hg}^{2+}$  remarkably quenched the emission intensity of ZrO<sub>2</sub>-8-HQS +  $\text{Zn}^{2+}$ . To find the quenching mechanism, the Stern–Volmer (SV) equation was used. The emission intensity quenches are related to the quencher concentration according to the following SV equation:

$$\left( \frac{\text{IF}_0}{\text{IF}} \right) = 1 + K_{\text{SV}}[\text{Q}] \quad (2)$$

Herein,  $\text{IF}_0$  is equal to the emission intensities in the absence of quenchers and  $\text{IF}$  is equal to the emission intensities in the quencher presentation. The slope of the SV equation,  $K_{\text{SV}}$ , is the SV constant, and  $[\text{Q}]$  is the quencher concentration. The modified SV equation is as follows:

$$\left( \frac{\text{IF}_0}{\text{IF}} \right) = (1 + K_{\text{S}}[\text{Q}]) (1 + K_{\text{D}}[\text{Q}]) \quad (3)$$

$K_{\text{S}}$  and  $K_{\text{D}}$  are represented as static and dynamic constants, respectively. Fig. S6† indicates the relative change in the emission intensities of ZrO<sub>2</sub>-8-HQS +  $\text{Zn}^{2+}$  as a function of quencher concentration. The concept of the SV quenching plot reveals that upward deviation from linearity indicates a combination of static and dynamic quenching, whereas no such deviation

indicates the occurrence of only one type of quenching mechanism.<sup>48</sup> According to the result, both dynamic and static quenching mechanisms are present in this system (Fig. 7). This conclusion is supported by the strong second-degree polynomial correlation observed between  $\text{IF}_0/\text{IF}$  (fitting data with modified SV equation) and the quencher concentration. The coefficient of determination ( $R^2$ ) exceeded 0.99, indicating an excellent fit between these variables. The  $(K_{\text{S}} \times K_{\text{D}})$  and  $(K_{\text{S}} + K_{\text{D}})$  values are 0.0012 and 0.0076, respectively.

To further evaluate the quenching mechanism of the optical probe, absorption spectroscopy was performed. The results indicated an isosbestic point at a wavelength of 333 nm following titration with  $\text{Hg}^{2+}$  (Fig. 7). Therefore, the quenching process allows the ZrO<sub>2</sub>-8-HQS +  $\text{Zn}^{2+}$  complex optical probe to detect  $\text{Hg}^{2+}$  selectively in aqueous solutions ( $\text{LoD} = 0.8 \mu\text{M}$ ). The interaction of  $\text{Hg}^{2+}$  with ZrO<sub>2</sub>-8-HQS +  $\text{Zn}^{2+}$  occurred rapidly within the first 10 seconds and showed no significant change over 300 seconds, as depicted in Fig. S7.† Table 3 demonstrates the comparison of various sensors that detect  $\text{Hg}^{2+}$  reported in previous studies with that demonstrated in this work.

### 3.3. pH effect

To investigate the pH effects on the as-prepared solid-state optical chemo-probe, a wide range of pH values from 2 to 10 were studied. Fig. S8† illustrates the result of optical chemo-probe performance in the sensing of  $\text{Zn}^{2+}$  ion in a wide pH range. According to the result, the as-prepared probe had good performance in various pH values from 4 to 10. Under harsh acidic conditions, the intensity of the chemo-probe was completely quenched (close to zero). At pH from 2 to 3, the intensity of the probe is approximately the same as fresh ZrO<sub>2</sub>-8-HQS. Therefore, this optical probe is unable to work under harsh acidic conditions. At pH = 4, the intensity enhanced to about 688, but above this pH, the intensity of the chemo-probe had not changed significantly.

## 4. Conclusion

In summary, upcycling valuable waste materials can pave the way for preventing the loss of important resources by converting them into high-value-added materials for use in specific applications. In this study, a facile and highly selective optical probe for  $\text{Zn}^{2+}$  in an aqueous environment was developed by upcycling



WBDPs with 8-HQS. The results clearly confirm that the prepared optical probe could selectively detect  $Zn^{2+}$  with a significant enhancement at  $\lambda_{em} = 517$  nm. Furthermore, the as-prepared optical probe could operate within a wide range of pH with high sensitivity. Through the competitive test with various ions, it was observed that  $Hg^{2+}$  caused quenching effects. It allows the  $Zn^{2+}$  optical complex to detect  $Hg^{2+}$  in aqueous media. Therefore, upcycling waste materials to create high-value-added substrates, such as solid-state optical chemoprobes, can contribute to sustainable development.

## Data availability

The data supporting this article have been included as part of the ESI.†

## Conflicts of interest

There are no conflicts to declare.

## References

- 1 D. Sajwan, A. Sharma, M. Sharma and V. Krishnan, Upcycling of Plastic Waste Using Photo-, Electro-, and Photoelectrocatalytic Approaches: A Way toward Circular Economy, *ACS Catal.*, 2024, **14**, 4865–4926.
- 2 X. Zhao, B. Boruah, K. F. Chin, M. Đokić, J. M. Modak and H. S. Soo, Upcycling to Sustainably Reuse Plastics, *Adv. Mater.*, 2022, **34**, 2100843.
- 3 L. Ou, R. Li, H. Zhu, H. Zhao and R. Chen, Upcycling waste phosphogypsum as an alternative filler for asphalt pavement, *J. Cleaner Prod.*, 2023, **420**, 138332.
- 4 R. Yousefi, S. Ahmadi, G. Mohammadi Ziarani and A. Badiei, Synthesis of  $[Ta_6O_19]$  @MOF composite as a chloroacetaldehyde optical sensor in wastewater obtained from two waste-resourced precursors: Tantalum from capacitors and terephthalic acid from PET bottle, *Mater. Today Sustain.*, 2023, **24**, 100604.
- 5 T. M. B. Campos, C. dos Santos, L. M. M. Alves, E. B. Benalcazar-Jalkh, H. B. Strazzi-Sahyon, E. T. P. Bergamo, S. M. Tebcherani, L. Witek, P. G. Coelho, S. Yamaguchi, G. P. Thim and E. A. Bonfante, Minimally processed recycled yttria-stabilized tetragonal zirconia for dental applications: Effect of sintering temperature on glass infiltration, *J. Mech. Behav. Biomed. Mater.*, 2024, **150**, 106311.
- 6 C. Siligardi, S. Barbi, R. Casini, L. Tagliaferri and V. Remigio, Recycling of yttria-stabilized zirconia waste powders in glazes suitable for ceramic tiles, *Int. J. Appl. Ceram. Technol.*, 2017, **14**, 1236–1247.
- 7 Y. Yang, J. Jiang, G. Shen and R. Yu, An optical sensor for mercury ion based on the fluorescence quenching of tetra(*p*-dimethylaminophenyl)porphyrin, *Anal. Chim. Acta*, 2009, **636**, 83–88.
- 8 X. Wang, Q. Lin, S. Ramachandran, G. Pembouong, R. B. Pansu, I. Leray, B. Lebental and G. Zucchi, Optical chemosensors for metal ions in aqueous medium with polyfluorene derivatives: Sensitivity, selectivity and regeneration, *Sens. Actuators, B*, 2019, **286**, 521–532.
- 9 S. Chakraborty, V. Ravindran, P. V. Nidheesh and S. Rayalu, Optical Sensing of Copper and Its Removal by Different Environmental Technologies, *ChemistrySelect*, 2020, **5**, 10432–10474.
- 10 Q. Li, T. Wang, Y. Jin, C. Wierzbicka, F. Wang, J. Li and B. Sellergren, Synthesis of highly selective molecularly imprinted nanoparticles by a solid-phase imprinting strategy for fluorescence turn-on recognition of phospholipid, *Sensor. Actuator. B Chem.*, 2022, **368**, 132193.
- 11 J. Krämer, R. Kang, L. M. Grimm, L. De Cola, P. Picchetti and F. Biedermann, Molecular Probes, Chemosensors, and Nanosensors for Optical Detection of Biorelevant Molecules and Ions in Aqueous Media and Biofluids, *Chem. Rev.*, 2022, **122**, 3459–3636.
- 12 G. Gigi and A. M. Mohan, Probe-impregnated monolithic polymer as a robust solid-state colorimetric chemosensor for selective sensing of  $Hg^{2+}$  in environmental water and cigarette samples, *Environ. Res.*, 2023, **220**, 115210.
- 13 J. Khan, Optical Chemosensors Synthesis and Application for Trace Level Metal Ions Detection in Aqueous Media: A Review, *J. Fluoresc.*, 2024, 1–22.
- 14 V. K. Gupta, A. K. Singh, L. K. Kumawat and N. Mergu, An easily accessible switch-on optical chemosensor for the detection of noxious metal ions  $Ni(II)$ ,  $Zn(II)$ ,  $Fe(III)$  and  $UO_2(II)$ , *Sens. Actuators, B*, 2016, **222**, 468–482.
- 15 J.-H. Hu, J.-B. Li, J. Qi and Y. Sun, Acylhydrazone based fluorescent chemosensor for zinc in aqueous solution with high selectivity and sensitivity, *Sens. Actuators, B*, 2015, **208**, 581–587.
- 16 K. H. Alharbi, A Review on Organic Colorimetric and Fluorescent Chemosensors for the Detection of  $Zn(II)$  Ions, *Crit. Rev. Anal. Chem.*, 2023, **53**, 1472–1488.
- 17 S. Das, M. Das, A. Bag, S. Laha, B. Chandra Samanta, I. Choudhury, N. Bhattacharya and T. Maity, Selective recognition of  $Zn(II)$  by a novel Schiff base chemosensor with the formation of an AIE active  $Zn(II)$  complex having picric acid detection ability: Application in live cell imaging study, *J. Photochem. Photobiol. Chem.*, 2024, **447**, 115214.
- 18 M. Budri, G. Naik, S. Patil, P. Kadolkar, K. Gudasi and S. Inamdar, A novel switch on and reversible optical sensor as an efficient, selective receptor for  $Zn(II)$  ion and its biological application, *Spectrochim. Acta Mol. Biomol. Spectrosc.*, 2020, **224**, 117462.
- 19 S. H. Mashraqui, R. Betkar, S. Ghorpade, S. Tripathi and S. Britto, A new internal charge transfer probe for the highly selective detection of  $Zn(II)$  by means of dual colorimetric and fluorescent turn-on responses, *Sens. Actuators, B*, 2012, **174**, 299–305.
- 20 M. Sohrabi, M. Amirsasr, S. Meghdadi, M. Lutz, M. Bikhof Torbati and H. Farrokhpour, A highly selective fluorescence turn-on chemosensor for  $Zn^{2+}$ , and its application in live cell imaging, and as a colorimetric sensor for  $Co^{2+}$ : experimental and TD-DFT calculations, *New J. Chem.*, 2018, **42**, 12595–12606.



21 J. Mishra, R. Kaur, A. K. Ganguli and N. Kaur, Urea/thiourea based dipodal nanoreceptors: Aqueous medium fluorescent chemosensor for Zn(II) and Hg(II) ions by photoinduced electron transfer, *Microchem. J.*, 2024, **206**, 111501.

22 V. Venkatesan, S. A. Kumar and S. K. Sahoo, Highly selective turn-on fluorogenic chemosensor for Zn<sup>2+</sup> based on chelation enhanced fluorescence, *Inorg. Chem. Commun.*, 2019, **102**, 171–179.

23 D. Paderni, L. Giorgi, M. Voccia, M. Formica, L. Caporaso, E. Macedi and V. Fusi, A New Benzoxazole-Based Fluorescent Macroyclic Chemosensor for Optical Detection of Zn<sup>2+</sup> and Cd<sup>2+</sup>, *Chemosensors*, 2022, **10**, 188.

24 V. Kumar, D. Singh, P. Kumar, G. Chaudhary, A. P. Singh and R. Gupta, Turn-on fluorescent detection of nickel and zinc ions by two related chemosensors containing naphthalimide ring(s), *J. Mol. Struct.*, 2022, **1261**, 132901.

25 A. Kolbus, A. Danel, P. Moskwa, K. Szary and T. Uchacz, Pyrazoloquinoline-based fluorescent sensor for the detection of Pb<sup>2+</sup>, Zn<sup>2+</sup> and the realization of an OR-type optical logic gate, *Dyes Pigm.*, 2024, **223**, 111956.

26 P. Srinivasan, S. P. Sivaraman, A. M. Mohan, D. K. Madhu, P. K. Chinaraga, C. B. Rao, S. Nagarajan and P. Deivasigamani, Chromoionophoric molecular probe infused bimodal porous polymer rostrum as solid-state ocular sensor for the selective and expeditious optical sensing of ultra-trace toxic mercury ions, *J. Hazard. Mater.*, 2024, **478**, 135483.

27 Z. Ruan, X. Dong, T. Long, S. Liu, Y. Chen and J. Lin, A novel fluorescent chemosensor enables dual-channel selective “turn-on” detection of Hg<sup>2+</sup> and Ag<sup>+</sup> via distinct thiophilic effects, essential mechanisms, and excellent sensing performance for mercury(ii) in aggregated states, *J. Mater. Chem. C*, 2024, **12**, 7572–7579.

28 C. Bissani Gasparin and D. A. Pilger, 8-Hydroxyquinoline, Derivatives and Metal-Complexes: A Review of Antileukemia Activities, *ChemistrySelect*, 2023, **8**, e202204219.

29 K. Soroka, R. S. Vithanage, D. A. Phillips, B. Walker and P. K. Dasgupta, Fluorescence properties of metal complexes of 8-hydroxyquinoline-5-sulfonic acid and chromatographic applications, *Anal. Chem.*, 1987, **59**, 629–636.

30 Rohini, K. Paul and V. Luxami, 8-Hydroxyquinoline Fluorophore for Sensing of Metal Ions and Anions, *Chem. Rec.*, 2020, **20**, 1430–1473.

31 A. I. Rabee, G. A. Mekhemer, A. Osatiashvili, M. A. Isaacs, A. F. Lee, K. Wilson and M. I. Zaki, Acidity-Reactivity Relationships in Catalytic Esterification over Ammonium Sulfate-Derived Sulfated Zirconia, *Catalysts*, 2017, **7**, 204.

32 H. Seo, M. K. Jackl, M. Kalaj and S. M. Cohen, Developing Metal-Binding Isosteres of 8-Hydroxyquinoline as Metalloenzyme Inhibitor Scaffolds, *Inorg. Chem.*, 2022, **61**, 7631–7641.

33 Z. H. Syed, M. R. Mian, R. Patel, H. Xie, Z. Pengmei, Z. Chen, F. A. Son, T. A. Goetjen, A. Chapovetsky, K. M. Fahy, F. Sha, X. Wang, S. Alayoglu, D. M. Kaphan, K. W. Chapman, M. Neurock, L. Gagliardi, M. Delferro and O. K. Farha, Sulfated Zirconium Metal-Organic Frameworks as Well-Defined Supports for Enhancing Organometallic Catalysis, *J. Am. Chem. Soc.*, 2022, **144**, 16883–16897.

34 H. Jianbo, Z. Tingting, C. Yongjing, Z. Yuanyuan, Y. Weiqing and M. Menglin, Study on Relationship Between Fluorescence Properties and Structure of Substituted 8-Hydroxyquinoline Zinc Complexes, *J. Fluoresc.*, 2018, **28**, 1121–1126.

35 M. H. Zare and A. Mehrabani-Zeinabad, Photocatalytic activity of ZrO<sub>2</sub>/TiO<sub>2</sub>/Fe<sub>3</sub>O<sub>4</sub> ternary nanocomposite for the degradation of naproxen: characterization and optimization using response surface methodology, *Sci. Rep.*, 2022, **12**, 10388.

36 M. Tao, S. Ishikawa, T. Ikeda, S. Yasumura, K. Shimoda, R. Osuga, Y. Jing, T. Toyao, K.-i. Shimizu, H. Matsuhashi and W. Ueda, Acid Catalysis over Crystalline Zr<sub>3</sub>SO<sub>9</sub>: Role of the Local Structure in Generating Acidity, *ACS Catal.*, 2023, **13**, 4517–4532.

37 L. Wu, A. C. Sedgwick, X. He and T. D. James, *Fluorescent Chemosensors*, Royal Society of Chemistry, 2023.

38 M. Khatun, P. Ghorai, J. Mandal, S. Ghosh Chowdhury, P. Karmakar and A. Saha, Design and synthesis of a hydrazinophthalazine derived chemosensor to detect metal ions Zn<sup>2+</sup>, Al<sup>3+</sup> via CHEF effect with biological study and theoretical calculation, *J. Photochem. Photobiol. Chem.*, 2024, **446**, 115145.

39 H. Xu, W. Chen, W. Zhang, L. Ju and H. Lu, A selective purine-based fluorescent chemosensor for the “naked-eye” detection of zinc ions (Zn<sup>2+</sup>): applications in live cell imaging and test strips, *New J. Chem.*, 2020, **44**, 15195–15201.

40 N. Honnappa, A. G. Anil, S. Shekar, S. K. Behera and P. C. Ramamurthy, Design of a Highly Selective Benzimidazole-Based Derivative for Optical and Solid-State Detection of Zinc Ion, *Inorg. Chem.*, 2022, **61**, 15085–15097.

41 D. Sarkar, A. K. Pramanik and T. K. Mondal, Coumarin based dual switching fluorescent ‘turn-on’ chemosensor for selective detection of Zn<sup>2+</sup> and HSO<sup>4-</sup>: an experimental and theoretical study, *RSC Adv.*, 2014, **4**, 25341–25347.

42 J.-c. Qin, L. Fan, B.-d. Wang, Z.-y. Yang and T.-r. Li, The design of a simple fluorescent chemosensor for Al<sup>3+</sup>/Zn<sup>2+</sup> via two different approaches, *Anal. Methods*, 2015, **7**, 716–722.

43 K. Kumarasamy, Z.-W. Wu, W.-J. Chien, M.-C. Lin and S. K. Ramasamy, A ratiometric turn-on chemosensor for highly selective and sensitive visual detection of Zn<sup>2+</sup> and its applications to environmental samples, *J. Environ. Chem. Eng.*, 2024, **12**, 114615.

44 S. Bari, D. Mridha, T. Roychowdhury and P. Roy, Detection of Zn<sup>2+</sup> and its imaging in plant roots by a bisphenol A-Based fluorescent chemosensor, *Inorg. Chim. Acta*, 2024, **566**, 122011.

45 R. Behura, P. P. Dash, P. Mohanty, S. Behera, M. Mohanty, R. Dinda, S. K. Behera, A. K. Barick and B. R. Jali, A Schiff base luminescent chemosensor for selective detection of Zn<sup>2+</sup> in aqueous medium, *J. Mol. Struct.*, 2022, **1264**, 133310.



46 M. Budri, G. Naik, S. Patil, P. Kadolkar, K. Gudasi and S. Inamdar, An ESIPT blocked highly ICT based molecular probe to sense Zn (II) ion through turn on optical response: Experimental and theoretical studies, *J. Photochem. Photobiol. A*, 2020, **390**, 112298.

47 S. Enbanathan, S. Munusamy, D. Jothi, S. Manojkumar, S. Manickam and S. K. Iyer, Zinc ion detection using a benzothiazole-based highly selective fluorescence "turn-on" chemosensor and its real-time application, *RSC Adv.*, 2022, **12**, 27839–27845.

48 A. S. Tanwar, R. Parui, R. Garai, M. A. Chanu and P. K. Iyer, Dual "Static and Dynamic" Fluorescence Quenching Mechanisms Based Detection of TNT via a Cationic Conjugated Polymer, *ACS Meas. Sci. Au*, 2022, **2**, 23–30.

49 A. Kumar, N. Ahmad, Y. Jadeja, S. Ganesan, J. Abd Hamid, P. Singh, K. Kaur and L. Hassen jaseem, Fluorescence sensor for mercury ions in aqueous mediums based on reduced graphene oxide linked with molybdenum disulfide, *J. Phys. Chem. Solids*, 2025, **196**, 112305.

50 Z. Liu, Z. Mo, X. Niu, X. Yang, Y. Jiang, P. Zhao, N. Liu and R. Guo, Highly sensitive fluorescence sensor for mercury(II) based on boron- and nitrogen-co-doped graphene quantum dots, *J. Colloid Interface Sci.*, 2020, **566**, 357–368.

51 H. Yang, L. Sun, H. Yu, A. P. Nugraha, J. R. V. Sáenz and G. Hong, Current prospect of dental zirconia recycling: A scoping review, *J. Prosthodont Res.*, 2024, **68**, 522–531.

52 M. Lan, J. Zhang, Y.-S. Chui, P. Wang, X. Chen, C.-S. Lee, H.-L. Kwong and W. Zhang, Carbon Nanoparticle-based Ratiometric Fluorescent Sensor for Detecting Mercury Ions in Aqueous Media and Living Cells, *ACS Appl. Mater. Interfaces*, 2014, **6**, 21270–21278.

53 M. Banerjee, M. Ghosh, S. Ta, J. Das and D. Das, A smart optical probe for detection and discrimination of  $Zn^{2+}$ ,  $Cd^{2+}$  and  $Hg^{2+}$  at nano-molar level in real samples, *J. Photochem. Photobiol. Chem.*, 2019, **377**, 286–297.

54 K.-H. Chu, Y. Zhou, Y. Fang, L.-H. Wang, J.-Y. Li and C. Yao, Rhodamine–pyrene conjugated chemosensors for ratiometric detection of  $Hg^{2+}$  ions: Different sensing behavior between a spirolactone and a spirothiolactone, *Dyes Pigm.*, 2013, **98**, 339–346.

55 B. Sen, M. Mukherjee, S. Pal, K. Dhara, S. K. Mandal, A. R. Khuda-Bukhsh and P. Chattopadhyay, A water soluble FRET-based ratiometric chemosensor for  $Hg^{(II)}$  and  $S^{2-}$  applicable in living cell staining, *RSC Adv.*, 2014, **4**, 14919–14927.

56 D. Aydin and I. Yilmaz, Simple synthesis and sensing applications of a new and low cost fluorescent chemosensor for selective recognition and facile removal of  $Hg^{2+}$ , *J. Photochem. Photobiol. Chem.*, 2021, **414**, 113280.

